RSC Advances

PAPER

View Article Online
View Journal | View Issue

Cite this: *RSC Adv.*, 2017, **7**, 2650

Co-immobilization of 1-vinyl-3-octadecylimidazolium cations and *p*-styrenesulphonate anions on silica and their anti-interference performance for the adsorption of naphthols†

Zhike Wang,*[a] Cunling Ye,[b] Lingyun Chen[a] and Haili Wu[a]

Adsorptive removals of naphthols are often interfered by some coexisting anions of aqueous solutions. In this work, 1-vinyl-3-octadecylimidazolium cations and *p*-styrenesulphonate anions were chemically co-modified on silica (denoted as Sil-PImC$_{18}$-SS) *via* the click chemistry reaction and were characterized. This material was created with the aim to explore the feasibility of removal of 1-naphthol (1-NAP) and 2-naphthol (2-NAP) from aqueous solutions. The prepared Sil-PImC$_{18}$-SS was used as an adsorbent to remove 1-NAP and 2-NAP from aqueous solutions and the effects of various variables for the adsorption of 1-NAP and 2-NAP were systematically studied. Among the coexisting anions tested, 0.2 mol L^{-1} background NaCl or Na_2SO_4 aqueous solutions had no significant effect on the adsorption of 1-NAP and 2-NAP. The adsorption behaviors of 1-NAP and 2-NAP were well described by the pseudo-second order kinetic and the Dubinin–Radushkevich models with the maximum adsorption capacities of 84.4 mg g^{-1} and 71.9 mg g^{-1} for 1-naphthol and 2-naphthol, respectively. The adsorption was a spontaneous and exothermic process, and an adsorption mechanism was speculated to be the cooperative contributions from the hydrophobic interaction, hydrogen bonding interaction, and π–π stacking. Thus, Sil-PImC$_{18}$-SS can be potentially used as an effective adsorption material for naphthol pollutant removal from the water environment.

Received 30th October 2016
Accepted 24th November 2016

DOI: 10.1039/c6ra26028d

www.rsc.org/advances

Introduction

1-Naphthol (1-NAP) and 2-naphthol (2-NAP) are position isomers and differ in the location of the hydroxyl group on the carbon skeleton of naphthalene. Since naphthols are widely used as raw materials or intermediates in many chemical industries, such as dyes, pigments, pharmaceuticals, pesticides, plastics, and synthetic rubber, they are present in the waste effluents discharged from these industries.[1] Moreover, naphthols are formed in the environment by the biodegradation of phenanthrene and Reactive Red 2.[2,3] 1-NAP and 2-NAP often coexist in wastewaters, have detrimental effects on the environment and human health, and have been considered as ubiquitous environmental carcinogens.[4,5] Naphthols, as persistent organic pollutants, are resistant to environmental degradation through biological, chemical or photolytic processes. Therefore, the removal of naphthols from wastewater will be of great significance.

There are a number of separation methods for naphthol removal including biodegradation, photodegradation, wet air oxidation, ozone degradation, adsorption, and other methods.[6–9] Among these, adsorption has gained more and more attention due to its low-cost, high efficiency, and easy operation. As a result, many adsorbents, such as activated carbon,[10] carbon black,[11] carbon nanotubes (CNTs),[7] graphene, graphene oxide and reduced graphene oxide (RGO),[1,12] bamboo hydrochars,[13] and montmorillonite,[14] have been investigated. In recent years, polymeric ionic liquids (PILs) prepared from ionic liquid (IL) monomers combine the unique properties of ILs together with intrinsic polymer characteristics, such as thermal and chemical stability, improved processability, durability, and spatial controllability.[15] Based on these advantages, PILs have been immobilized on different supports, such as silicas,[16] RGO,[17] CNTs,[18] metal–organic frameworks (MOFs),[19] and polyhedral oligomeric silsesquioxanes (POSSs),[20] for various specific applications. The preparation methods for these PILs-grafted materials mainly include the immobilization of only cation monomers, anion monomers, or both on the supports.[16] In particular, for the immobilization of only anion or cation monomers of ILs on the supports, ion exchange easily happens between their corresponding counter

[a]*School of Environment, Henan Key Laboratory for Environmental Pollution Control, Key Laboratory for Yellow River and Huai River Water Environment and Pollution Control, Ministry of Education, Henan Normal University, Xinxiang, Henan 453007, P. R. China. E-mail: wzk@htu.cn; Tel: +86-373-3325971*

[b]*School of Chemistry and Chemical Engineering, Henan Normal University, Xinxiang, Henan 453007, P. R. China*

† Electronic supplementary information (ESI) available. See DOI: 10.1039/c6ra26028d

Table 1 Selected physicochemical properties of 1-NAP and 2-NAP[a22–25]

Adsorbate	Chemical structure	S	log K_{OW}	pK_a
1-NAP		6.00	2.85	9.34
2-NAP		6.94	2.71	9.5

[a] S: aqueous solubility, mmol L^{-1}; K_{OW}: n-octanol–water partition coefficient; pK_a: acid dissociation constant.

ions and other ionic species in the explored medium, whereas co-immobilization can avoid this exchange. In other words, these PILs-grafted materials prepared by the co-immobilization method can have the ability to suppress the interferences of ionic species in water environments in terms of adsorbents;[21] to date, little research on the use of these co-immobilization materials as adsorbents to remove the pollutants from water environments has been reported.

Considering the inherent properties of 1-NAP and 2-NAP, such as weak acidity, hydrophobicity, and aromaticity (Table 1),[22–25] there is a chance of the removal of naphthols from the aqueous solutions using the co-immobilized PILs-modified silica adsorbents due to their tunable selectivity and multiple beneficial physical characteristics towards the target adsorbate, and the interferences coming from the anions in water environments for adsorption can be simultaneously inhibited. Theoretically, 1-vinyl-3-octadecylimidazolium cations should provide most types of interactions, including strong hydrophobic interactions, π–π stacking, hydrogen bonding, and electrostatic interactions, whereas p-styrenesulphonate anions exhibit additional π–π interactions. Thus, Sil-PImC_{18}-SS prepared from 1-vinyl-3-octadecylimidazolium cation and p-styrenesulphonate anion monomers should exhibit good adsorption performance for 1-NAP and 2-NAP. In this study, the main objective was to explore the feasibility of removal of 1-NAP and 2-NAP from the aqueous solutions using Sil-PImC_{18}-SS as the adsorbent and to elucidate the adsorption mechanism. The effects of various parameters, such as pH, initial concentrations of 1-NAP and 2-NAP, temperature, contact time, and ionic strength, were investigated in detail. Kinetics, isotherm models, and thermodynamics of the adsorption were also studied.

Experimental

Materials

1-Vinylimidazole (99%), 1-bromooctadecane (97%), sodium p-styrenesulphonate (90%), 3-mercaptopropyltrimethoxysilane (95%), 1-NAP, and 2-NAP were purchased from Aladdin Chemistry Co. Ltd. Azobisisobutyronitrile (AIBN) was obtained from Guangfu Institute of Fine Chemicals (Tianjin, China) and purified by recrystallization from methanol before use. Silica gel (200–300 mesh), 2-nitrophenol (2-NP), 3-nitrophenol (3-NP), 4-nitrophenol (4-NP) and 2,4-dinitrophenol (2,4-DNP), toluene, chloroform, and acetonitrile were obtained from Sinopharm Chemical Reagent Co., Ltd. (Shanghai, China) and the solvents were further dried before use. Dry toluene was obtained by distillation after toluene was dried with calcium chloride and further dried by standing with sodium. Dry chloroform was obtained by distillation after drying over calcium chloride and anhydrous calcium sulfate. Dry acetonitrile was obtained by distillation after drying with anhydrous calcium chloride and phosphoric anhydride.

Preparation of Sil-PImC_{18}-SS

According to the reported studies,[16] the synthesis method includes four steps. First, 1-vinyl-3-octadecylimidazolium bromide ([C_{18}VIm]Br) was synthesized. 1-Bromooctadecane (18.33 g) was dissolved in dry acetonitrile, and then 4.71 g 1-vinylimidazole was added dropwise. After this, the mixture was mixed at 60 °C for three days. [C_{18}VIm]Br was obtained after being recrystallized in cold diethyl ether and dried under vacuum for 12 h at 30 °C.

Second, 1-vinyl-3-octadecylimidazolium p-styrenesulphonate ([C_{18}VIm]SS) was synthesized by the exchange of bromide to p-styrenesulphonate. [C_{18}VIm]Br (5 g) and sodium p-styrenesulphonate (2.5 g) were dissolved in 50 mL water. The mixture was mixed at room temperature for two days. After this, white [C_{18}VIm]SS was obtained after being washed with water and dried under vacuum at 30 °C.

Third, mercaptopropyl-modified silica (Sil-MPS) was prepared. Silica gel was first activated by immersing in 6 mol L^{-1} hydrochloric acid for 24 h, and then washed with water and dried at 100 °C for 12 h. Activated silica gel (6 g) was dispersed in 30 mL dry toluene and 3 g 3-mercaptopropyltrimethoxysilane was added dropwise. The mixture was mixed for 36 h at 125 °C. The obtained Sil-MPS was washed in turn with toluene, methanol, water, methanol and diethyl ether, and then dried for 12 h at 60 °C.

Finally, 1-vinyl-3-octadecylimidazolium p-styrenesulphonate was immobilized onto the silica surface *via* the click chemistry reaction between the vinyl groups of 1-vinyl-3-octadecylimidazolium p-styrenesulphonate and thiol groups of Sil-MPS. Sil-MPS (2.8 g) and [C_{18}VIm]SS (2 g) were dissolved in 30 mL dry chloroform, and then 0.02 g AIBN was added. After this, the mixture was mixed under nitrogen atmosphere for 30 h at 60 °C. Then, the adsorbent, Sil-PImC_{18}-SS, was obtained after being washed with chloroform, methanol, and diethyl ether. The detailed preparation procedure is described in Fig. S1.†

Characterization

Elemental analyses were carried out using a Vario EL elemental analyzer (Germany). Two parallel analyses were made for each material. The surface morphology was examined using a scanning electron microscope (JEOL, JSM-6390 LV). The Fourier transform infrared (FTIR) spectra were obtained using a Perkin-Elmer-983 IR spectrophotometer in the range of 400–4000 cm^{-1}. Thermogravimetric analysis (STA449C, Netzsch, Germany) was performed with a heating rate of 10 °C min^{-1} under nitrogen. N_2 adsorption–desorption experiments were carried out using a Quantachrome NOVA 2000e sorption analyzer at

liquid nitrogen temperature (77 K). The specific surface area (S_{BET}) was estimated by the linear part of the Brunauer–Emmett–Teller (BET) equation, and the pore size distribution was calculated by the Barrett–Joyner–Halenda (BJH) method. The UV-visible spectra of Sil-PImC_{18}-SS before and after the adsorption of 1-NAP and 2-NAP were obtained using a Lambda 950 UV/vis/NIR spectrophotometer (Perkin Elmer).

Adsorption experiments

An aqueous solution of 1-NAP or 2-NAP was freshly prepared by dissolving 1-NAP or 2-NAP in deionized water. Negligible volumes of 0.1 mol L^{-1} HCl or 0.1 mol L^{-1} NaOH aqueous solutions were used to adjust the pH value of the aqueous solutions. The adsorption behaviors of 1-NAP and 2-NAP on the adsorbent were investigated using a conventional batch equilibrium technique. A predetermined amount of an adsorbent and 50 mL aqueous solutions with different 1-NAP or 2-NAP concentrations was added to 100 mL conical flasks that were shaken for 5 h to ensure complete adsorption in a THZ-82(A) thermostatic water-bath shaker at 160 rpm (Jintan Scientific Analytical Instrument Co. Ltd., China). After adsorption for a predetermined time, the adsorbent was removed from the mixture by filtration. The concentrations of 1-NAP or 2-NAP in the supernatant were analyzed by a UV/visible spectrophotometer (UV-5100, Shanghai Metash Instruments Co. Ltd., China) at the appropriate optimum UV wavelengths of 293 and 327 nm for 1-NAP and 2-NAP, respectively. The adsorbed amounts of 1-NAP or 2-NAP were calculated by eqn (1).

$$Q_e = (C_0 - C_e)V/W \quad (1)$$

where Q_e (mg g^{-1}) is the equilibrium adsorption capacity of 1-NAP or 2-NAP on the adsorbent. C_0 and C_e are the initial concentration and the equilibrium concentration of 1-NAP or 2-NAP, respectively. V (L) presents the volume of the solution and W (g) is weight of the adsorbent.

Blank experiments without 1-NAP or 2-NAP were simultaneously carried out to correct the results. In addition, control experiments containing 1-NAP or 2-NAP without the adsorbent were carried out to evaluate the solute losses. The experimental results showed that such losses were negligible.

Results and discussion

Characterization of Sil-PImC_{18}-SS

The elemental compositions of Sil-MPS and Sil-PImC_{18}-SS were C: 5.01%, H: 1.66%; and C: 27.49%, H: 4.39%, N: 1.81%, respectively. Compared to Sil-MPS, the percentages of carbon for Sil-PImC_{18}-SS increased from 5.01% to 27.49%, and this increase in the carbon percentage (22.48%) should be attributed to the successful copolymerization of 1-vinyl-3-octadecylimidazolium *p*-styrenesulphonate onto the silica substrate. The C/N ratio was 12.42, which was almost equal to the initial C/N ratio (13.28) for 1-vinyl-3-octadecylimidazolium *p*-styrenesulphonate. This indicated that the anion and cation of 1-vinyl-3-octadecylimidazolium *p*-styrenesulphonate were simultaneously copolymerized to Sil-MPS with a ratio of 1 : 1. The elemental analysis data proved that the immobilization on the surface was successful.

The surface morphologies of the activated silica, Sil-MSP, and Sil-PImC_{18}-SS were examined by SEM. As observed in Fig. 1, the surface of the activated silica was relatively smooth; however, Sil-MSP possessed a rough surface. The image of Sil-PImC_{18}-SS showed a granular structure, suggesting that the PILs were successfully grafted onto the surface of activated silica. The FTIR spectra of activated silica, Sil-MSP, and Sil-PImC_{18}-SS are shown in Fig. S2.† The typical peaks of Si–O–Si were observed around 802 and 1100 cm^{-1}. For activated silica, the characteristic peak at 970 cm^{-1} was attributed to the presence of silanol groups. For Sil-MSP, the peak at 970 cm^{-1} disappeared, which indicated that the silanol groups had reacted with 3-mercaptopropyltrimethoxysilane. The peak at 689 cm^{-1} means the presence of C–S. The peak around 2934 cm^{-1} was assigned to the C–H stretches of tetrahedral carbon. For the Sil-PImC_{18}-SS, the peak at 1008 cm^{-1} indicated the presence of sulfonate group. The peaks around 2923 and 2853 cm^{-1} were due to the C–H stretching of the long alkyl chain. The peaks near 1412, 1472, and 1639 cm^{-1} were attributed to the aromatic benzene, and the peak around 1565 cm^{-1} indicated the presence of the imidazole ring. From the FTIR spectrum, it can be concluded that the cation and anion of 1-vinyl-3-octadecylimidazolium *p*-styrenesulphonate were successfully copolymerized onto the silica.

N_2 adsorption–desorption experiments were performed at 77 K (Fig. 2). Compared with activated silica, a significant decrease

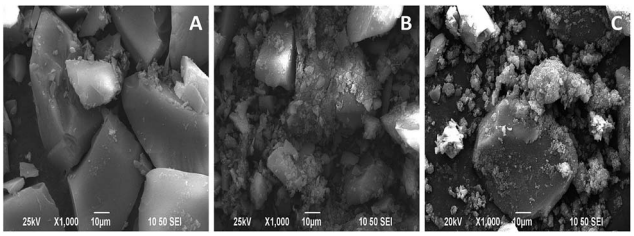

Fig. 1 SEM images of activated silica (A), Sil-MSP (B), and Sil-PImC_{18}-SS (C).

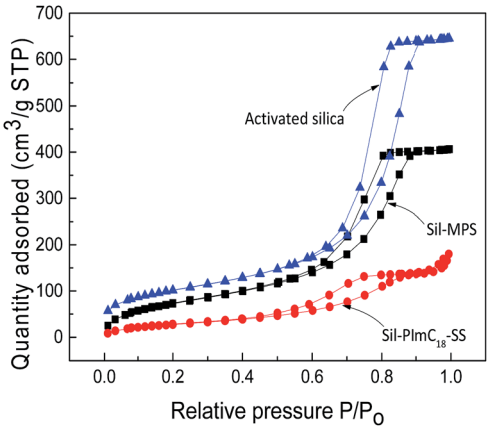

Fig. 2 N_2 adsorption/desorption isotherms of activated silica, Sil-MSP, and Sil-PImC_{18}-SS.

Table 2 Textural properties of activated silica, Sil-MSP, and Sil-PImC$_{18}$-SS

Materials	BET surface area (m^2 g^{-1})	Volume of pore (cm^3 g^{-1})	Average pore diameter (nm)
Activated silica	357.6	0.9995	9.6625
Sil-MSP	278.4	0.6126	7.2690
Sil-PImC$_{18}$-SS	107.8	0.2729	7.9228

in the BET surface area and pore volume of Sil-MPS was observed (Table 2). Moreover, compared with Sil-MPS, the BET surface area and pore volume of Sil-PImC$_{18}$-SS significantly decreased. Thus, compared with activated silica, the average pore diameter of Sil-MPS and Sil-PImC$_{18}$-SS significantly decreased. The decrease in the porosity was attributed to the extra bulk of 1-vinyl-3-octadecylimidazolium styrenesulfonate.

The thermogravimetric curves for activated silica, Sil-MPS, and Sil-PImC$_{18}$-SS are presented in Fig. S3.† For activated silica, the mass loss in the region from 200 to 800 °C was 2.9%, which can be attributed to the condensation of silanol groups. For Sil-MPS, a higher mass loss between 200 and 800 °C was observed (14.5%), which can be attributed to the loss of mercaptopropyl attached to the surfaces of silica. Compared with Sil-MPS, the mass losses between 200 and 800 °C increased from 14.5% to 40.9%; the increase in the mass loss was attributed to the successful immobilization of 1-vinyl-3-octadecylimidazolium *p*-styrenesulphonate onto the silica surface.

Adsorption properties of activated silica and Sil-PImC$_{18}$-SS

The adsorption of 1-NAP and 2-NAP onto activated silica and Sil-PImC$_{18}$-SS is presented in Fig. 3. It can be seen from the figure that the amount of adsorption of Sil-PImC$_{18}$-SS for 1-NAP and 2-NAP significantly increased as compared to that of activated silica. Fig. 4 further compares the UV-visible spectra of Sil-PImC$_{18}$-SS before and after the adsorption of 1-NAP and 2-NAP, respectively. It was obvious that the characteristic adsorption peak of 1-NAP (298 nm) and 2-NAP (331 nm) appeared after

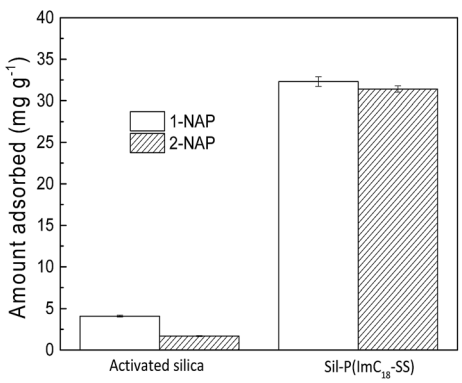

Fig. 3 Comparison of the adsorption performance of activated silica and Sil-PImC18-SS (experimental conditions: volume of aqueous solution, 50 mL; initial concentration, 50 mg L^{-1}; adsorbent mass, 30 mg; shaking speed, 160 rpm; shaking time, 5 h; and temperature, 30 °C).

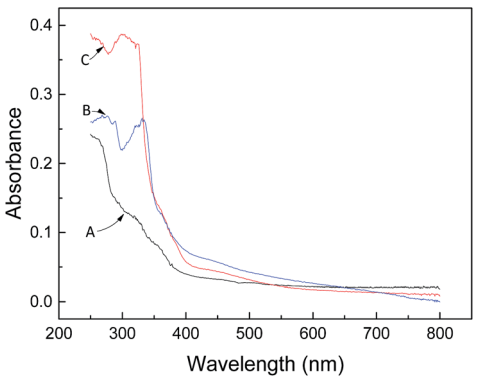

Fig. 4 UV-visible spectra of Sil-PImC18-SS before (A) and after the adsorption of 1-NAP (C) and 2-NAP (B).

adsorption; this phenomenon indicated that 1-NAP and 2-NAP could be efficiently adsorbed onto Sil-PImC$_{18}$-SS.

Selectivity of Sil-PImC$_{18}$-SS

To investigate the selectivity of Sil-PImC$_{18}$-SS, 2-NP, 3-NP, 4-NP, and 2,4-DNP were used as adsorbates. The adsorption experiments were performed in 50 mL of 50 mg L^{-1} of each nitrophenols aqueous solutions containing 30 mg of Sil-PImC$_{18}$-SS and shaken at a constant speed of 160 rpm at 30 °C for 5 h. The obtained Q_e was 11.3, 10.6, 10.2, and 9.6 mg g^{-1} for 2-NP, 3-NP, 4-NP, and 2,4-DNP, respectively. Compared with the Q_e of Sil-PImC$_{18}$-SS for 1-NAP and 2-NAP, the four nitrophenols demonstrated lower adsorption amounts. This could be attributed to their different molecular structures. They all have a hydroxyl group on their individual molecular structure. For 1-NAP and 2-NAP, there are two benzene rings. For these nitrophenols, they not only have one benzene ring, but also contain an electron-withdrawing nitro functional group that decreases the electron density of the aromatic ring. The smaller electron density in the aromatic ring supplies less π-electrons to interact with the adsorbent, and accordingly, accounts for the lower amount of adsorption for the four nitrophenols on Sil-PImC$_{18}$-SS as compared to that of 1-NAP or 2-NAP.

Effect of pH

Adsorptions of 1-NAP and 2-NAP on Sil-PImC$_{18}$-SS were carried out in the pH range of 2–11. As can be seen in Fig. 5, the adsorption of 1-NAP on Sil-PImC$_{18}$-SS exhibited the same trend as that of 2-NAP, and the adsorption capacities of 1-NAP and 2-NAP slightly decreased at pH < 8, whereas these obviously decreased at pH > 9.[26] For weakly acidic compounds, such as 1-naphthol and 2-naphthol, the occurrence of their non-dissociated and dissociated species depends on the pH value of the aqueous solution and their dissociation constants (pK_a). The content of nondissociated and dissociated species can be calculated according to eqn (2) and (3), respectively.

$$f_N = 1/(1 + 10^{pH-pK_a}) \quad (2)$$

$$f = 1/(1 + 10^{pK_a-pH}) \quad (3)$$

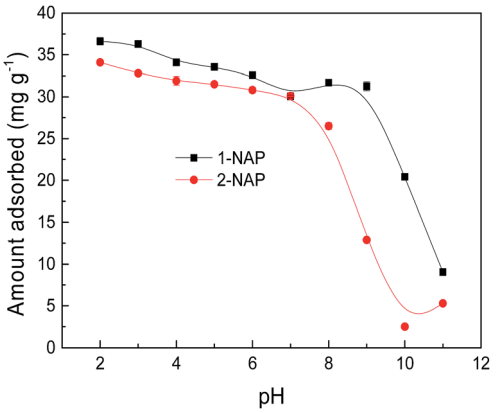

Fig. 5 Effect of pH on the adsorption of 1-NAP and 2-NAP.

where f_N and f are the content of the nondissociated and dissociated species, respectively. The distributions of the non-dissociated and dissociated species for 1-NAP and 2-NAP in the aqueous solution were predicted as a function of solution pH values and are shown in Fig. S4,† respectively. 1-NAP and 2-NAP adsorption on Sil-PImC_{18}-SS exhibited the same trend as that of the dissociation curves of 1-NAP and 2-NAP in the aqueous solution, which displayed that the molecular states of 1-NAP and 2-NAP were suitable for the adsorption, whereas the ionic states were not suitable. Moreover, the adsorption capacity of 1-NAP on Sil-PImC_{18}-SS was larger than that of 2-NAP in the investigated pH range. According to the experimental results, octanol–water partition coefficient, and water solubility of 1-NAP and 2-NAP (shown in Table 1), it can be concluded that the larger K_{OW} and the smaller solubility would benefit the naphthol adsorption onto Sil-PImC_{18}-SS. This adsorption phenomenon was attributed to the possible hydrophobic interactions, hydrogen bonding interactions (N atoms of imidazolium as the hydrogen bonding acceptors and –OH of naphthols as donors), and π–π stacking between Sil-PImC_{18}-SS and 1-NAP and 2-NAP.[27] The adsorbent, Sil-PImC_{18}-SS, not only has a long octadecyl chain to increase the hydrophobicity, but also contains imidazolium groups to incorporate the hydrogen bonding interactions and π–π stacking. The naphthols, 1-NAP and 2-NAP, not only have two benzene rings to increase the hydrophobicity, but also contain a –OH group to incorporate the hydrogen bonding interactions. The hydroxyl groups are strong electron donors that make the naphthalene ring of 1-NAP and 2-NAP become π-electron rich, thus facilitating π–π interactions between the naphthalene ring of 1-NAP and 2-NAP and the phenyl and imidazolium rings of Sil-PImC_{18}-SS. At high pH, –OH group of 1-NAP and 2-NAP would be ionized and their polarity would increase. Thus, the hydrophobic interactions between anionic 1-NAP and 2-NAP and the adsorbent would be significantly weakened. At the same time, hydrogen bonding interactions between the –OH group of 1-NAP and 2-NAP (as donors) and the N-containing group of Sil-PImC_{18}-SS (as acceptors) would also be significantly impeded due to the ionization of the –OH group of 1-NAP and 2-NAP. Therefore, the adsorption capacities of 1-NAP and 2-NAP on Sil-PImC_{18}-SS decreased with the increase of pH value.

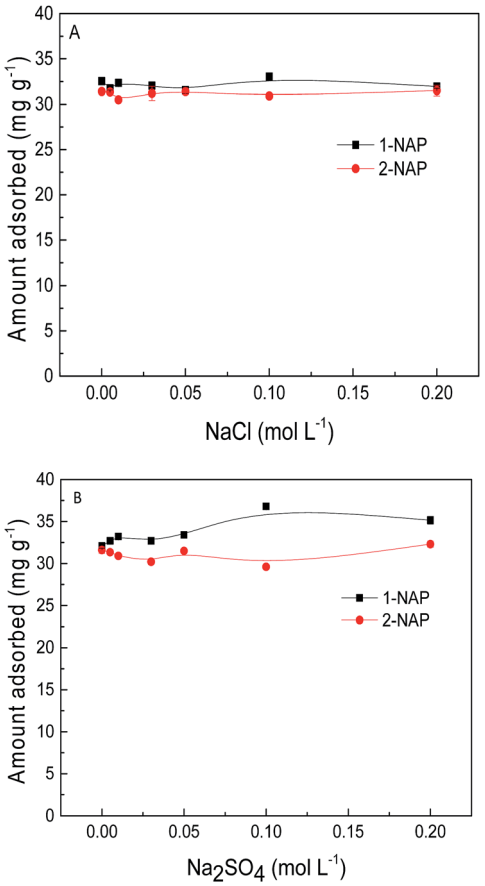

Fig. 6 Effect of ionic strength ((A) NaCl and (B) Na_2SO_4) on the adsorption of 1-NAP and 2-NAP.

Effect of coexisting anions

1-NAP and 2-NAP are always present in waste water with some other ionic species, especially anions, which can affect the adsorption performance of Sil-PImC_{18}-SS.[28] Therefore, the effect of inorganic salts, such as NaCl and Na_2SO_4, on the adsorption ability of Sil-PImC_{18}-SS for 1-NAP and 2-NAP from aqueous solutions was investigated, and the results are depicted in Fig. 6. Fig. 6 shows that the adsorption of 1-NAP and 2-NAP was not affected when the background NaCl and Na_2SO_4 concentration increased from 0 to 0.2 mol L^{-1}.

The excellent adsorption performance of Sil-PImC_{18}-SS for 1-NAP and 2-NAP under high ionic strength was attributed to the cooperative contributions of hydrophobic, hydrogen bonding, and π–π interactions.

Adsorption kinetics

The adsorption of 1-NAP and 2-NAP by Sil-PImC_{18}-SS over different contact times was investigated, as presented in Fig. 7. It can be seen that the adsorption equilibrium was reached within 300 min and no significant change was observed from 300 to 540 min. Therefore, a contact time of 300 min was selected for the sure establishment of the adsorption equilibrium in the further adsorption experiments. To evaluate the adsorption kinetics of 1-NAP and 2-NAP onto Sil-PImC_{18}-SS, the

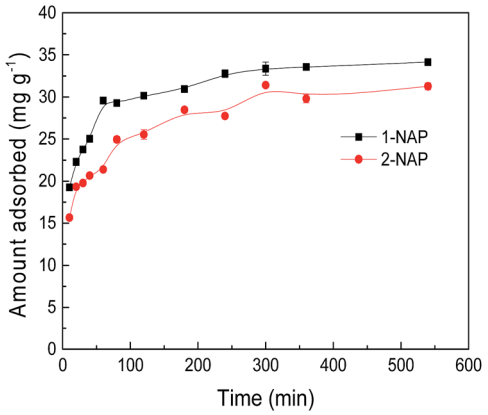

Fig. 7 Effect of contact time on the adsorption of 1-NAP and 2-NAP.

kinetic data were further statistically investigated using the pseudo-first order, pseudo-second order, and intra-particle kinetic models, as shown in eqn (4), (5) and (6), respectively.[29,30]

$$\ln(Q_e - Q_t) = \ln Q_e - k_1 t \quad (4)$$

$$t/Q_t = 1/(Q_e^2 k_2) + t/Q_e \quad (5)$$

$$Q_t = k_3\sqrt{t} + C \quad (6)$$

where Q_e and Q_t are the adsorption capacities at equilibrium and at time t, respectively (mg g^{-1}). k_1 (min^{-1}), k_2 (g mg^{-1} min^{-1}), and k_3 (mg g^{-1} $min^{-1/2}$) are the pseudo-first order rate constant, pseudo-second order rate constant, and the diffusion rate constant, respectively. C (mg g^{-1}) is a constant.

The values of Q_e and k_2 can be calculated from the slopes and intercepts of the pseudo-second order kinetic plots using eqn (5). When $t \rightarrow 0$, the initial adsorption rate, h, can be defined as eqn (7).

$$h = k_2 Q_e^2 \quad (7)$$

Table 3 summarizes the corresponding model parameters. The correlation coefficients suggest that the adsorption process was most suitably fitted by the pseudo-second order equation (R^2: 0.9993 for 1-NAP, 0.9931 for 2-NAP) when compared to the pseudo-first order equation (R^2: 0.9612 for 1-NAP, 0.8493 for 2-NAP) and the intra-particle kinetic equation (R^2: 0.7432 for 1-NAP, 0.9166 for 2-NAP). Moreover, the calculated equilibrium adsorption capacities ($Q_{e,cal}$: 34.1 mg g^{-1} for 1-NAP, 34.4 mg g^{-1} for 2-NAP) were close to the experimental values.

Table 3 Kinetic parameters for the adsorption of 1-NAP and 2-NAP[a]

Models	Parameters	1-NAP	2-NAP
Pseudo-first order model	$Q_{e,exp}$ (mg g^{-1})	34.2	34.7
	k_1 (min^{-1})	0.0089	0.0034
	$Q_{e,cal}$ (mg g^{-1})	12.4	14.9
	R^2	0.9612	0.8493
Pseudo-second order model	k_2 (g mg^{-1} min^{-1})	0.0026	0.0009
	$Q_{e,cal}$ (mg g^{-1})	34.1	34.4
	h (mg g^{-1} min^{-1})	3.0168	1.0894
	R^2	0.9993	0.9931
Intra-particle diffusion model	k_3 (mg g^{-1} $min^{-1/2}$)	0.5627	0.7317
	C (mg g^{-1})	20.8	15.9
	R^2	0.7432	0.9166

[a] ($Q_{e,exp}$: 34.2 mg g^{-1} for 1-NAP, 34.7 mg g^{-1} for 2-NAP), which further confirmed the applicability of the pseudo-second order rate equation for the adsorption of 1-NAP and 2-NAP onto Sil-PImC_{18}-SS.

Adsorption isotherms

Fig. 8 shows the adsorption isotherms of 1-NAP and 2-NAP onto Sil-PImC_{18}-SS. The equilibrium adsorption data were analyzed by the most common Langmuir (eqn (8)) and Freundlich (eqn (9)) models.[31,32]

$$Q_e = bC_eQ_m/(1 + bC_e) \quad (8)$$

$$Q_e = K_F C_e^{1/n} \quad (9)$$

where C_e (mg L^{-1}) is the 1-NAP or 2-NAP concentration at equilibrium, Q_e (mg g^{-1}) is the equilibrium adsorption capacity of 1-NAP or 2-NAP by the adsorbent, Q_m is the monolayer adsorption capacity (mg g^{-1}), b is the Langmuir constant, K_F and $1/n$ are the constants (indicative of the relative adsorption capacity of the adsorbent and the constant indicative of the heterogeneity factor of the Freundlich adsorption isotherm, respectively).

The relative parameters calculated from the Langmuir and Freundlich models are presented in Table 4. According to the

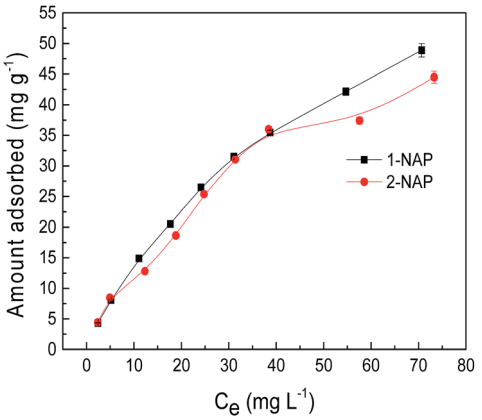

Fig. 8 Adsorption isotherms of 1-NAP and 2-NAP.

Table 4 Langmuir, Freundlich, and Dubinin–Radushkevich isotherm constants

Models	Parameters	1-NAP	2-NAP
Langmuir	Q_m (mg g^{-1})	84.4	71.9
	b (L mg^{-1})	0.0189	0.0218
	R^2	0.9987	0.9748
Freundlich	K_F (mg g^{-1})(mg L^{-1})^n	3.3684	3.5332
	$1/n$	0.6343	0.5979
	R^2	0.9922	0.9577
Dubinin–Radushkevich	$Q_{m,DR}$ (mmol g^{-1})	3.407	2.6218
	K_{DR} (mol^2 kJ^{-2})	0.0062	0.0058
	E (kJ mol^{-1})	9.0112	9.3099
	R^2	0.9989	0.9841

Table 5 Q_m values of adsorbents reported in the literature for the adsorption of 1-NAP and 2-NAP

Adsorbents	Q_m (mg g^{-1}) 1-NAP	2-NAP	Reference
Sil-PImC_{18}-SS	84.4	71.9	This study
^{2}c-G-MWCNTs	37.74	—	7
Sludge-based activated carbon	—	111.9	10
GO/ARG/CRG	57.7–282	—	12
Anion–cation organopalygorskite	—	33.65	30
Oxidized MWCNTs	30.57	—	31
Fe_3O_4@polyaniline	28.74	9.13	33
Biochars of orange peels	27.07	—	34

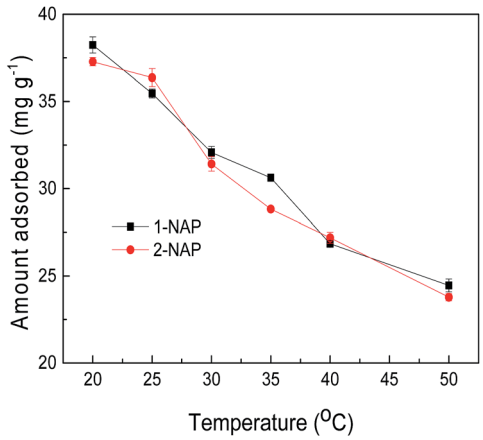

Fig. 9 Effect of temperature on the adsorption of 1-NAP and 2-NAP.

correlation coefficients, the adsorption isotherms fitted well with those of the Langmuir model. The maximum adsorption capacities (Q_m) fitted by the Langmuir model for 1-NAP and 2-NAP were 84.4 and 71.9 mg g^{-1}, respectively. Compared to the adsorption capacities of 1-NAP and 2-NAP on other reported adsorbents (Table 5), Sil-PImC_{18}-SS was a suitable material for the removal of 1-NAP and 2-NAP from the aqueous solutions.

The Dubinin–Radushkevich (D–R) isotherm model, as shown in eqn (10), was further applied to analyze the adsorption energy for deciding the nature of adsorption process as physical or chemical.[35,36]

$$\ln Q_{e,DR} = \ln Q_{m,DR} - K_{DR}\varepsilon^2 \quad (10)$$

where $Q_{e,DR}$ (mol g^{-1}) is the equilibrium adsorption capacity, $Q_{m,DR}$ (mol g^{-1}) and K_{DR} (mol^2 kJ^{-2}) are the D–R isotherm constants related to the capacity and free energy of adsorption, and ε (kJ mol^{-1}) is the Polanyi potential, which is equal to $RT\ln(1 + 1/C_{e,DR})$. R is the universal gas constant (8.314 J mol^{-1} K^{-1}), T is the absolute temperature (K), and $C_{e,DR}$ (mol L^{-1}) is the equilibrium concentration.

The free energy of adsorption E (kJ mol^{-1}) was calculated using the following equation:

$$E = 1\Big/\sqrt{2K_{DR}} \quad (11)$$

The parameters for the D–R model are shown in Table 4. The correlation coefficients of 1-NAP and 2-NAP were 0.9989 and 0.9841, respectively, which indicated that the adsorption of 1-NAP and 2-NAP onto Sil-PImC_{18}-SS fitted well with the D–R isotherm model. Moreover, the free energy of adsorption was higher than 8 kJ mol^{-1} for the adsorption of 1-NAP and 2-NAP, revealing that the adsorption process could be considered to be chemical adsorption.[37]

Thermodynamic analysis

Thermodynamic studies were performed to further elucidate the adsorption mechanism of 1-NAP or 2-NAP onto the adsorbent. As shown in Fig. 9, the adsorption of 1-NAP or 2-NAP continuously decreased as the temperature increased from 20 to 50 °C, which indicated that the adsorption process was an exothermic process and was favored at lower temperature. The thermodynamic parameters, such as Gibbs free energy change (ΔG), enthalpy change (ΔH), and entropy change (ΔS), were calculated by the following equations:[38,39]

$$K = Q_e/C_e \quad (12)$$

$$\Delta G = -RT\ln K \quad (13)$$

$$\ln K = \Delta S/R - \Delta H/RT \quad (14)$$

where K is the distribution coefficient.

As presented in Table 6, the values of ΔG and ΔH of the process at five temperatures were negative, indicating that the adsorption process was a spontaneous and exothermic process. The negative value of ΔS implied a decrease in the randomness at the solid/liquid interface due to the orderly adsorption of 1-NAP or 2-NAP.

Regeneration and reuse of Sil-PImC_{18}-SS

Desorption and reuse experiments were investigated through three consecutive cycles. After adsorption of 1-NAP and 2-NAP, the adsorbents were collected and fully washed with deionized

Table 6 Thermodynamic parameters for the adsorption of 1-NAP and 2-NAP

Adsorbates	ΔH (kJ mol^{-1})	ΔS (kJ mol^{-1} K^{-1})	ΔG (kJ mol^{-1}) 20 °C	25 °C	30 °C	35 °C	40 °C	50 °C
1-NAP	−19.27	−0.0056	−17.67	−17.64	−17.51	−17.61	−17.37	−17.56
2-NAP	−19.71	−0.0072	−17.56	−17.75	−17.42	−17.37	−17.42	−17.46

water. Then, 1-NAP and 2-NAP loaded Sil-PImC$_{18}$-SS was immersed in ethanol and stirred at 30 °C for 5 h. The Q_e of 1-NAP decreased a little from the initial value of 33.4 mg g^{-1} to 29.1 mg g^{-1} and the Q_e of 2-NAP ranged from 31.4 mg g^{-1} to 27.9 mg g^{-1} after three consecutive cycles. These results indicate that Sil-PImC$_{18}$-SS could be easily regenerated and have the potential for application in the removal of 1-NAP and 2-NAP from the aqueous solutions.

Conclusions

In this work, Sil-PImC$_{18}$-SS, with a good adsorption capacity for 1-NAP and 2-NAP, was prepared and characterized by elemental analysis, FTIR, SEM, N_2 adsorption–desorption experiments, and thermogravimetric analysis. The Sil-PImC$_{18}$-SS performed well over a wide pH range from 2 to 8. Importantly, Sil-PImC$_{18}$-SS also had a good adsorption performance for naphthols even in presence of some coexisting anions, such as Cl^- and SO_4^{2-}. The adsorption behavior could be fitted well with the Dubinin–Radushkevich model and pseudo-second order model. The adsorption of 1-NAP and 2-NAP onto the Sil-PImC$_{18}$-SS was a spontaneous and exothermic process and might be controlled by multiple mechanisms such as hydrophobic, hydrogen bonding, and π–π interactions. These results suggest that Sil-PImC$_{18}$-SS is a potentially efficient material for the removal of naphthols from water environment.

Acknowledgements

This work was supported by the National Natural Science Foundation of China (No. 21107022) and the Key Scientific Research Project of Higher Education of Henan Province of China (No. 15A610006).

Notes and references

1 M. M. Ali and K. Y. Sandhya, *RSC Adv.*, 2014, **4**, 51624–51631.
2 N. V. Balashova, I. A. Kosheleva, N. P. Golovchenko and A. M. Boronin, *Process Biochem.*, 1999, **35**, 291–296.
3 D. C. Kalyani, A. A. Telke, R. S. Dhanve and J. P. Jadhav, *J. Hazard. Mater.*, 2009, **163**, 735–742.
4 Y. Pang, Y. Zhang, W. Li, H. Ding and X. Shen, *J. Electroanal. Chem.*, 2016, **769**, 89–96.
5 X. Peng, H. Wang, B. Yang, X. Zhan and Y. Wu, *Chromatographia*, 2016, **79**, 327–333.
6 X. Wang, C. Chen, J. Li and X. Wang, *Chem. Eng. J.*, 2015, **262**, 1303–1310.
7 Z. Wu, H. Yang, F. Jiao, Q. Liu, X. Chen and J. Yu, *Colloids Surf., A*, 2015, **470**, 149–160.
8 M. Shiohara, T. Isobe, S. Matsushita and A. Nakajima, *Mater. Chem. Phys.*, 2016, **183**, 37–43.
9 L. Xu, J. Li and M. Zhang, *Ind. Eng. Chem. Res.*, 2015, **54**, 2379–2384.
10 L. Gu, Y. Wang, N. Zhu, D. Zhang, S. Huang, H. Yuan, Z. Lou and M. Wang, *Bioresour. Technol.*, 2013, **146**, 779–784.
11 L. Zuo, S. Yu, L. Cheng and E. Du, *Korean J. Chem. Eng.*, 2013, **30**, 714–723.
12 J. Wang and B. Chen, *Chem. Eng. J.*, 2015, **281**, 379–388.
13 Y. Li, A. Meas, S. Shan, R. Yang and X. Gai, *Bioresour. Technol.*, 2016, **207**, 379–386.
14 S. Yang, M. Gao, Z. Luo and Q. Yang, *Chem. Eng. J.*, 2015, **268**, 125–134.
15 L. Chen and X. Huang, *J. Chromatogr. A*, 2016, **1466**, 42–49.
16 H. Qiu, A. K. Mallik, T. Sawada, M. Takafuji and H. Ihara, *Chem. Commun.*, 2012, **48**, 1299–1301.
17 J. Liu, M. Wang, Y. Zhang, L. Han, X. Chen and J. Wang, *RSC Adv.*, 2014, **4**, 61936–61943.
18 Q. Wen, Y. Wang, K. Xu, N. Li, H. Zhang and Q. Yang, *Anal. Chim. Acta*, 2016, **939**, 54–63.
19 Z. Li, W. Wang, Y. Chen, C. Xiong, G. He, Y. Cao, H. Wu, M. D. Guiver and Z. Jiang, *J. Mater. Chem. A*, 2016, **4**, 2340–2348.
20 D. Lu, J. Zhao, Y. Leng, P. Jiang and C. Zhang, *Catal. Commun.*, 2016, **83**, 27–30.
21 J. Feng, M. Sun, L. Xu, S. Wang, X. Liu and S. Jiang, *J. Chromatogr. A*, 2012, **1268**, 16–21.
22 X. Yang, J. Li, T. Wen, X. Ren, Y. Huang and X. Wang, *Colloids Surf., A*, 2013, **422**, 118–125.
23 F. Wang, J. J. H. Haftka, T. L. Sinnige, J. L. M. Hermens and W. Chen, *Environ. Pollut.*, 2014, **186**, 226–233.
24 X. Sun, W. Huang, Z. Ma, Y. Lu and X. Shen, *J. Hazard. Mater.*, 2013, **252–253**, 192–197.
25 S. Yang, M. Gao, Z. Luo and Q. Yang, *Chem. Eng. J.*, 2015, **268**, 125–134.
26 C. He, J. Huang, C. Yan, J. Liu, L. Deng and K. Huang, *J. Hazard. Mater.*, 2010, **180**, 634–639.
27 J. Huang, B. Yuan, X. Wu and S. Deng, *J. Colloid Interface Sci.*, 2012, **380**, 166–172.
28 C. Sun, B. Xiong, Y. Pan and H. Cui, *J. Colloid Interface Sci.*, 2017, **487**, 175–181.
29 R. Li, C. Lin and X. Liu, *RSC Adv.*, 2016, **6**, 19872–19877.
30 Y. Tai, C. Shi and C. Wang, *J. Mol. Liq.*, 2014, **195**, 116–124.
31 G. D. Sheng, D. D. Shao, X. M. Ren, X. Q. Wang, J. X. Li, Y. X. Chen and X. K. Wang, *J. Hazard. Mater.*, 2010, **178**, 505–516.
32 S. Chaudhary, P. Sharma, Renu and R. Kumar, *RSC Adv.*, 2016, **6**, 62797–62809.
33 Q. Zhou, Y. Wang, J. Xiao and H. Fan, *Synth. Met.*, 2016, **212**, 113–122.
34 B. Chen and Z. Chen, *Chemosphere*, 2009, **76**, 127–133.
35 H. R. Nodeh and H. Sereshti, *RSC Adv.*, 2016, **6**, 89953–89965.
36 T. Zhao and T. Feng, *RSC Adv.*, 2016, **6**, 90878–90886.
37 Y. Seki, S. Seyhan and M. Yurdakoc, *J. Hazard. Mater.*, 2006, **138**, 60–66.
38 W. Huang, X. Yu and D. Li, *RSC Adv.*, 2015, **5**, 84937–84946.
39 S. Radi, S. Tighadouini, M. Bacquet, S. Degoutin, L. Janus and Y. N. Mabkhot, *RSC Adv.*, 2016, **6**, 82505–82514.